THE JOURNAL OF PHYSICAL CHEMISTRY B
A JOURNAL OF THE AMERICAN CHEMICAL SOCIETY

pubs.acs.org/JPCB

Article

Theoretical Analysis of the Role of Water in Ligand Binding to Cucurbit[*n*]uril of Different Sizes

Published as part of The Journal of Physical Chemistry virtual special issue "Hiro-o Hamaguchi Festschrift".

Natthiti Chiangraeng, Haruyuki Nakano, Piyarat Nimmanpipug,* and Norio Yoshida*

Cite This: *J. Phys. Chem. B* 2023, 127, 3651−3662

Read Online

ACCESS | Metrics & More | Article Recommendations | Supporting Information

ABSTRACT: The role of water in host−ligand binding was investigated using a combination of molecular dynamics simulation and three-dimensional reference interaction site model theory. Three different hosts were selected (CB6, CB7, and CB8). Six organic molecules were used as representative ligands: dimethyl sulfoxide (DMSO), *N*,*N*-dimethylformamide (DMF), acetone, 2,3-diazabicyclo[2.2.2]oct-2-ene (DBO), cyclopentanone (CPN), and pyrrole. From the binding free energy and its components, we divided the ligands into two groups: those with relatively small molecular size (DMSO, DMF, acetone, and pyrrole) and those with relatively large molecular size (DBO and CPN). We established that the solvent water in the CB6 cavity can be completely displaced by small ligands, resulting in a greater binding affinity compared with larger CBs, except in the case of the small pyrrole ligand, due to outstanding intrinsic properties such as the relatively high hydrophobicity and low dipole moment. In the case of the large ligands, the solvent water can be displaced by DBO and CPN in both CB6 and CB7; there were similar tendencies in their binding affinities, with the greatest affinity in the CB7 complexes. However, the tendencies of the binding affinity components are completely different due to the difference between the complex structure and the solvation structure when a ligand binds with a CB structure. The binding affinities suggest that the size fit between the ligand and CB cannot guarantee the greatest binding affinity gain because the binding structure and intrinsic properties of CB and ligand equally play a crucial role.

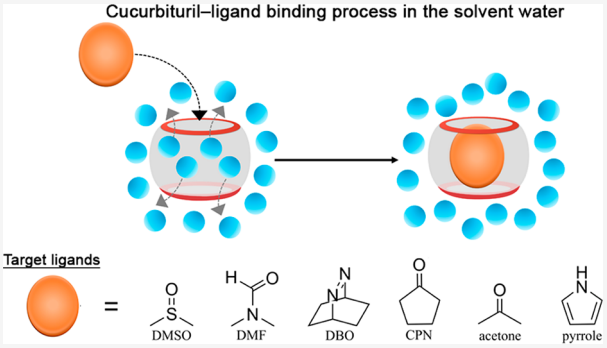

1. INTRODUCTION

Molecular recognition (MR) is one of the most fundamental processes in biological systems and has attracted much attention in the field of physics, chemistry, biochemistry, and drug/material design.[1,2] It is regarded as a process in which a ligand molecule binds within the cavity of a host molecule through noncovalent chemical bonds between host and ligand molecules, such as electrostatic interactions, hydrogen bonding, and van der Waals forces. Basically, this process is a fundamental mechanism of drug delivery systems.[1−4] MR also includes molecular aggregation and self-assembly, and it is the subject of research in a wide range of scientific fields.[5−7] MR is known as a stochastic process, governed by free energy change of the system. Therefore, it is important to consider not only the direct interaction between the host and ligand molecules but also the influence of surrounding environments in the MR process. For example, when MR occurs in an aqueous solution, dehydration of both the host and ligand molecules associated with ligand binding, and the resulting reorganization of the entire solvent system and change in translational entropy of the solvent, may play an important role. In other words, the generation of new hydrogen bonds by the dehydrated hydration water, resulting from the host−ligand binding, leads to a rearrangement (reorganization) of the hydrogen bond network of the surrounding solvent water. The ligand binding also changes the effective volume of translational movement of the solvent water, which in turn changes the translational entropy of the solvent.[8] Good knowledge of these aspects can aid researchers in the design of host−ligand complexes with high-affinity binding for specific applications.

Cucurbit[*n*]uril (CB*n*) is a macrocyclic compound that comprises *n* glycoluril monomers bridged by 2*n* methylene units leading to a hollow pumpkin shape as shown in Figure 1. There are two openings for in and/or out movement of the ligand and solvent molecules. CB structures have a hydrophobic cavity and contain many hydrophilic carbonyl groups around the cavity. Medium-sized CB, including CB6, CB7, and

Received: January 16, 2023
Revised: March 20, 2023
Published: April 18, 2023

https://doi.org/10.1021/acs.jpcb.3c00343
J. Phys. Chem. B 2023, 127, 3651−3662

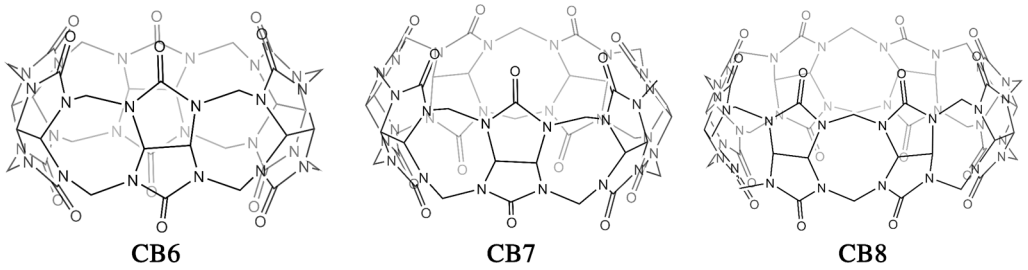

Figure 1. Structures of cucurbit[*n*]urils.

CB8, offers water solubility, and thus suitability for use in biological systems.[2,9,10] Therefore, CB−ligand complex formation via intermolecular interactions can be useful for drug design purposes.

CB−ligand binding systems have attracted much attention due to the various intrinsic properties of CB structures.[1,2] Their cavities can be varied, resulting in changes in the portal size, which can then lead to the formation of larger ligands of interest or involve more molecules inside the cavity.[1,4] Moreover, CB*n* has low toxicity and is biocompatible; its medicinal and pharmaceutical use has been suggested.[11−16]

In an aqueous solution, the CB pocket will be occupied by water molecules when no ligand molecule binds with the CB host. At this time, the ligands are solvated by the water molecules in solution. To form a complex, the ligand moves into the cavity of CB and displaces the water molecules. The ligand occupies the region inside the cavity due to superior intermolecular interactions. Subsequently, water molecules will move out from the cavity. A schematic of the CB−ligand binding process is illustrated in Figure 2.

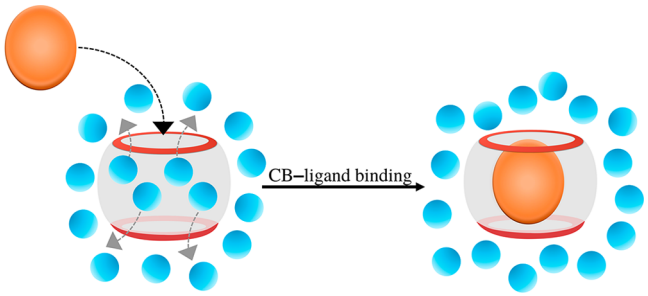

Figure 2. Schematic illustration of CB−ligand binding. The orange and blue beads represent ligand and water molecules, respectively. The cage represents the CB*n* host structure.

To date, many authors have utilized the continuum solvent model[4,17] and explicit solvent water in molecular dynamics (MD) simulations[18−21] to computationally study the behavior of CB−ligand binding systems in aqueous solution. In those studies, the essential role of solvent water has been pointed out. Grimm et al. examined the ligand binding affinity of CB7 and CB8 by experimental and computational methods and argued that the dominant factor in affinity is not the London dispersion interaction, nor the electronic energy or entropy factor, but the solvation effect specific to each host−ligand combination.[21] Biedermann et al. reported that solvent water molecules are essential in governing the CB−ligand binding.[18] The water molecules must be displaced from the CB pocket in the complexation process due to unfavorable binding compared with CB−ligand binding. Basically, the CB−ligand complex can be formed in water environments with high binding affinity because of the presence of high-energy water in the CB cavity.[21] The high-energy water was considered in terms of the energy of breaking hydrogen bonds between water molecules and the CB structure prior to forming a ligand of interest. They also suggested that hydrophobic ligands tend to provide greater binding affinities of the CB complex due to favorable hydrophobic−hydrophobic interactions between the ligand and the CB cavity. Moreover, they also investigated the CB7−receptor complex for analyte molecules with high selectivity.[19] They concluded that the high-energy water molecules are also key to a complexation driving force. However, as mentioned, the origin of the driving force governing complexation between CB*n* and ligand remains unclear.[2,18,19]

To elucidate the details of the CB−ligand binding mechanism, an integral equation theory of molecular liquids, such as the three-dimensional reference interaction site model (3D-RISM), may be effective because of its statistical mechanical treatment of the solvent environments.[3,22] As mentioned earlier, solvents play an essential role in the MR processes that occur in water. Statistical mechanics theory is the best way to evaluate hydration properties related to changes in the free energy of an entire system, such as solvation entropy and solvent reorganization.

The 3D-RISM theory is based on the statistical mechanics derived from the molecular Ornstein−Zernike equation.[23−28] This fundamental equation describes the pair correlation of liquids for a solute−solvent system at infinite dilution. The 3D-RISM theory was selected for use in this study because it has been successfully applied to study MR, and it provides reasonable results compared with the available data.[3] Moreover, 3D-RISM theory can handle the sampling method for the entire configuration space in a solution containing a number of water molecules. With this theory, the analytical method of configuration integration is performed over the whole system. This capability is a substantial advantage of 3D-RISM because it can overcome the sampling difficulties in conventional MD simulations. We can obtain the solvation structure from 3D-RISM calculations. Furthermore, it also handles explicit solvent water, to represent the reliability properties and phenomena of interest, which is different from typical simulations of the continuum solvent model. In addition, the simulations can account for the changes in a partial molar volume (PMV) and the solvation free energy (SFE)[29] because the theory can treat the reorganization of water molecules.[30] This is crucial for the investigations of solute−solvent and solvent−solvent interactions. According to Imai, analysis of the PMV can provide insight into the solvation effects of the host−ligand binding system, offering a better understanding.[31] The 3D-RISM theory is briefly described later in the text.

https://doi.org/10.1021/acs.jpcb.3c00343
J. Phys. Chem. B 2023, 127, 3651−3662

The accuracy of the SFE evaluated by the 3D-RISM theory is examined in many previous studies.[32−42] These studies have shown that the SFE formalism in 3D-RISM has been improved and is comparable in accuracy to experimental and MD data. For example, a comparison of SFEs between 3D-RISM with pressure correction, which employed in the present study, and MD performed for over 400 organic molecules by Sergiievskyi et al. showed that the mean error and its standard deviation were only −1.5 and 0.97 kcal mol^{-1}, respectively.[34] Taking advantage of these features, 3D-RISM has shown good performance in SAMPL5,[41] SAMPL6,[40] and SAMPL7,[39] and it has also been successfully applied to molecular recognition by supramolecules such as cyclodextrins.[43−45] Thus, 3D-RISM can be expected to be a suitable method for assessing the binding affinity of ligands by CBs.

Herein, the 3D-RISM theory was applied to study the CB−ligand binding in aqueous solution. We chose CB6, CB7, and CB8 as complex hosts in this study. Six organic molecules, namely dimethyl sulfoxide (DMSO), *N*,*N*-dimethylformamide (DMF), acetone, 2,3-diazabicyclo[2.2.2]oct-2-ene (DBO), cyclopentanone (CPN), and pyrrole, were used as representative ligands (as also mentioned by Biedermann et al.).[18] Our computational results, such as differences in binding free energy, were qualitatively compared with available experimental data.[18] To shed more light on the driving force for CB−ligand complexation, the internal energies, the SFEs, and their components were analyzed and described. The CB size dependencies of ligand binding affinities were systematically studied, and detailed results are presented.

2. METHODS AND COMPUTATIONAL DETAILS

2.1. Theoretical Framework. Here, we now briefly describe the equations related to the 3D-RISM theory that is utilized in our discussion. A more detailed explanation can be found elsewhere.[3,25,30,46,47] We assume that the CB and ligand molecules are in finite dilution in the solvent water molecules, and all solute and solvent molecules are treated by the RISM method.

The total free energy G can be expressed as

$$G = E_{\mathrm{mm}} + G_{\mathrm{solv}} \tag{1}$$

where E_{mm} and G_{solv} are the solute internal potential energy and SFE, respectively. Therefore, the binding free energy ΔG_{bind} can be defined as

$$\Delta G_{\mathrm{bind}} = \Delta E_{\mathrm{mm}} + \Delta G_{\mathrm{solv}} \tag{2}$$

The internal energy change ΔE_{mm} is calculated from MD simulation results as follows:

$$\Delta E_{\mathrm{mm}} = E_{\mathrm{complex}} - (E_{\mathrm{CB}} + E_{\mathrm{ligand}}) \tag{3}$$

where E_{CB}, E_{ligand}, and E_{complex} are the internal energies with respect to CB*n*, ligand, and CB*n*−ligand complex, respectively. In the RISM method, the change in SFE ΔG_{solv} can be given by

$$\Delta G_{\mathrm{solv}} = G_{\mathrm{solv}}^{\mathrm{complex}} - (G_{\mathrm{solv}}^{\mathrm{CB}} + G_{\mathrm{solv}}^{\mathrm{ligand}}) \tag{4}$$

where $G_{\mathrm{solv}}^{\mathrm{CB}}$, $G_{\mathrm{solv}}^{\mathrm{ligand}}$, and $G_{\mathrm{solv}}^{\mathrm{complex}}$ are the SFEs with respect to CB*n*, ligand, and the CB*n*−ligand complex, respectively.

In our study, the Kovalenko−Hirata (KH) closure was utilized to solve unknown functions,[25] including total and direct correlation functions, in the RISM equations. This closure's advantages are well-known, and the convergence is well behaved and sufficiently treated in finite dilution systems. With this closure, the thermodynamic properties related to the solvation effect can be readily obtained from the standard thermodynamic derivative of the free energy.[48−50] In RISM calculations, the interaction potential between every solute and solvent site is treated by conventional Lennard-Jones (LJ) and electrostatic interaction potentials. This can be written as

$$u_\gamma(\boldsymbol{r}) = \sum_\alpha 4\varepsilon_{\alpha\gamma}\left[\left(\frac{\sigma_{\alpha\gamma}}{|\boldsymbol{r}-\boldsymbol{r}_\gamma|}\right)^{12} - \left(\frac{\sigma_{\alpha\gamma}}{|\boldsymbol{r}-\boldsymbol{r}_\gamma|}\right)^{6} + \frac{1}{4\pi\varepsilon_0}\frac{q_\alpha q_\gamma}{|\boldsymbol{r}-\boldsymbol{r}_\gamma|}\right] \tag{5}$$

where $\varepsilon_{\alpha\gamma}$ and $\sigma_{\alpha\gamma}$ are the LJ energy and size parameters for a pair of solute α and solvent sites γ, respectively, ε_0 is the dielectric constant in the vacuum, and q is the effective partial charges in each site.

The PMV ($\Delta\bar{V}$) is an important quantity to investigate the effective molecular volume in solution. $\Delta\bar{V}$ of the solute in the finite dilution can be calculated using the Kirkwood−Buff equation generalized to the interaction site representation of liquid and solutions as shown[48]

$$\Delta\bar{V} = k_{\mathrm{B}}T\chi_T\left[1 - \rho\sum_\gamma C_\gamma(\boldsymbol{r})\,\mathrm{d}\boldsymbol{r}\right] \tag{6}$$

where χ_T is the isothermal compressibility of the solution obtained from the site−site correlation function.

2.2. Molecular Dynamics Simulation. We performed MD simulations using AMBER20 software.[51] Before running the MD simulation, the initially isolated structures of CB*n* and ligands were optimized with HF/6-31G(d) calculations in vacuum using the Gaussian16 software[52] to prepare initial structures and effective point charges for MD simulations. The effective point charges were evaluated based on the restrained electrostatic potential (RESP) charge method. The potential parameters in the MD simulation were assigned according to the general Amber force field (GAFF) procedure via the Antechamber tool.[53] In this study, we chose the TIP3P[54] for water molecules in the explicit solvent water. The tleap module was used to generate topology and coordinate input files for all structures. About 2500 water molecules were added to hydrate the CBs and their complexes, while about 1500 water molecules were added in the case of the free ligands. The corresponding cuboid box volume is approximately 100,000 and 60,000 Å^3, respectively. In this study, we made use of six ligands: DMSO, DMF, acetone, DBO, CPN, and pyrrole (see Figure 3). The molecular properties of the ligands are summarized in Table 1.

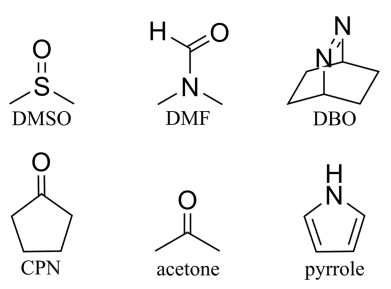

Figure 3. Structures of ligands used in this study.

https://doi.org/10.1021/acs.jpcb.3c00343
J. Phys. Chem. B 2023, 127, 3651−3662

Table 1. Dipole Moment μ Calculated from the Partial Charges, Octanol–Water Partition Coefficient log K_{ow}, and Empirical Parameters of Solvent Polarity $E_T(30)$

ligand	dipole moment (debye)[a]	log K_{ow}	$E_T(30)$ (kcal mol^{-1})
DMSO	4.77	−1.35[55]	45.1,[56] 45.0[57]
DMF	4.40	−1.01[58]	43.2,[56] 43.8[57]
DBO	3.87	3.27[b], 1.76[c]	N/A
CPN	3.31	0.38[59]	39.4,[56] 43.0[57]
acetone	3.19	−0.24[55,59]	42.2[56,57]
pyrrole	1.89	0.75[55]	51.0[60]

[a]Values obtained from the partial charge determined by the RESP procedure. [b]Data provided in https://www.chemspider.com/Chemical-Structure.121537.html. [c]Data provided in https://www.chemeo.com/cid/24-739-5/2-3-Diazabicyclo-2-2-2-oct-2-ene.

The PMEMD module was used in energy minimization, while the GPU-accelerated PMEMD code[61−63] was utilized in MD simulation steps. Initially, each model was minimized sequentially using the steepest descent method of 5000 cycles and the conjugate gradient method of 5000 cycles to prepare the suitable structures. Thereafter, the isothermal–isobaric ensemble was carried out at 300 K and 1 bar for 500 ns, with a time step of 0.002 ps. The equilibrium state was run for 100 ns, while the rest of the time is the production state. The temperature and pressure were controlled by the Berendsen thermostat and barostat,[64] respectively. The SHAKE method[65] was applied to constrain bond lengths involving hydrogen atoms. All 2000 snapshots were extracted from the MD trajectory and utilized for further analysis; they were subsequently used as initial structures for 3D-RISM runs.

2.3. Three-Dimensional Reference Interaction Site Model Calculation. In this part, the CB and ligand were treated as solute molecules in 3D-RISM calculations. All explicit water molecules were stripped from the MD snapshot before carrying out 3D-RISM calculations. The 3D-RISM was utilized in our system at the limit of finite dilution. The KH closure[25] was chosen due to the rapid convergence attained.[24,66] We set the number of grid points to 128^3, with a grid spacing of 0.5 Å. All 3D-RISM calculations were carried out using in-house 3D-RISM packages developed by our group.[67−69]

3. RESULTS AND DISCUSSION

3.1. Solvation Properties of CBs and Ligands. Prior to discussing the binding process, the solvation properties of CBs and ligands were investigated in aqueous solution.

In Figure S1, the root-mean-square deviations (RMSDs) of heavy atoms in CBs during the MD simulation are depicted. The RMSDs of CB6 and CB7 remained low throughout the entire MD trajectory. By contrast, the variation in RMSD of CB8 with time indicated two stable structures. In Figure S2a, the representative structures of CB8 in each state are shown. Since the initial structure of the CB8 for MD simulation takes a circular form, the structures of lower RMSD have a circular form, while those of higher RMSD have an elliptical form. As the trajectory and the thermodynamic properties in Figure S2b,c show, the elliptical form is only a few kcal mol^{-1} more stable than the circular one, so these structures are likely to be in equilibrium. In the discussion that follows, we used averaged values over the trajectory, including both forms.

The SFEs of the CBs increase negatively with an increasing number of glycoluril units (see Figure 4a). This is because the

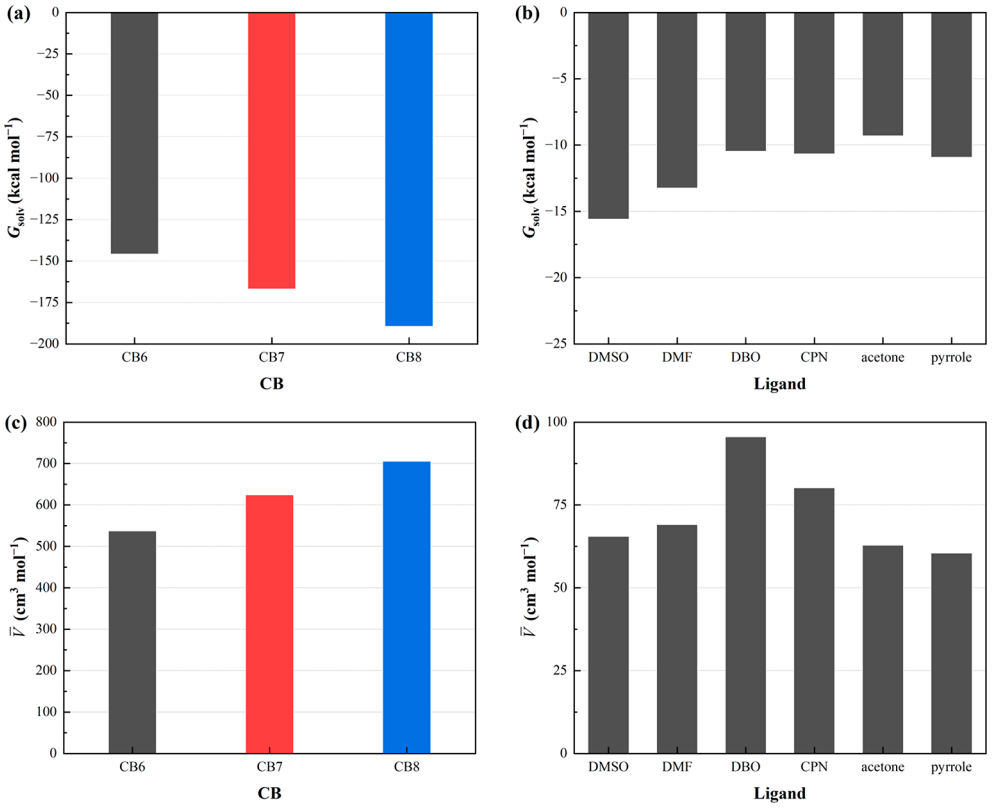

Figure 4. Solvation free energy (G_{solv}) and $\bar{V}$ of (a, c) CBs and (b, d) ligands, respectively.

https://doi.org/10.1021/acs.jpcb.3c00343
J. Phys. Chem. B 2023, 127, 3651−3662

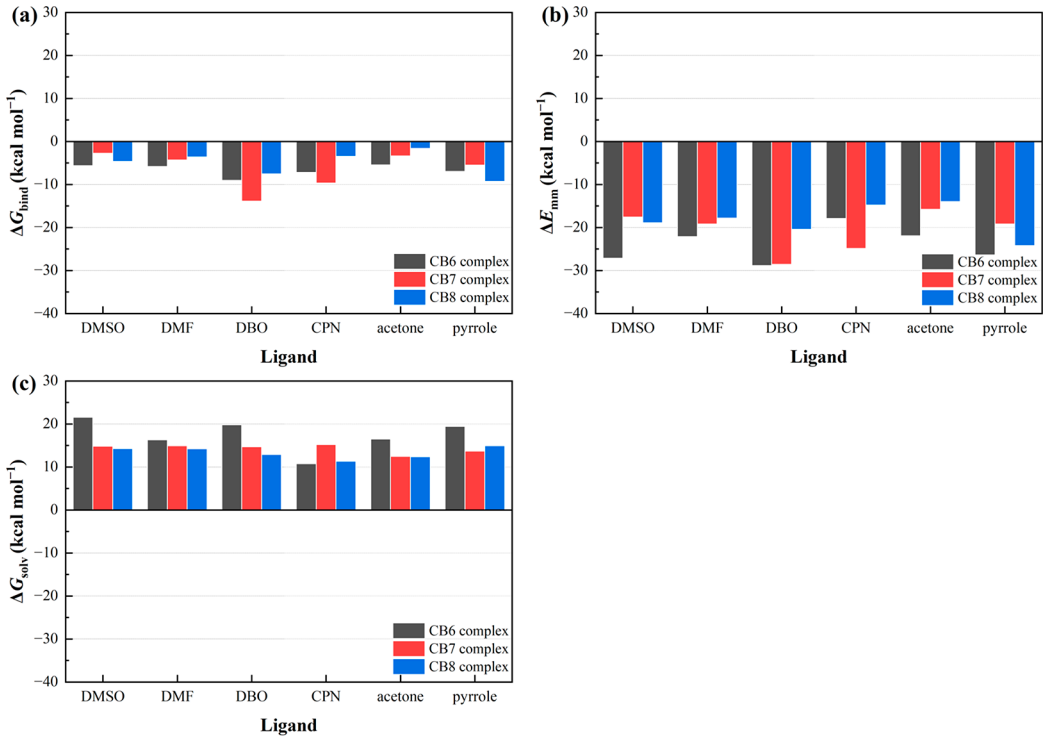

Figure 5. Binding free energy and its components for all combinations of CBs and ligands. (a) Total binding free energy ΔG_{bind}, (b) solute structural and interaction energy change ΔE_{mm}, and (c) solvation free energy change ΔG_{solv}. All the values are given in kcal mol^{-1}.

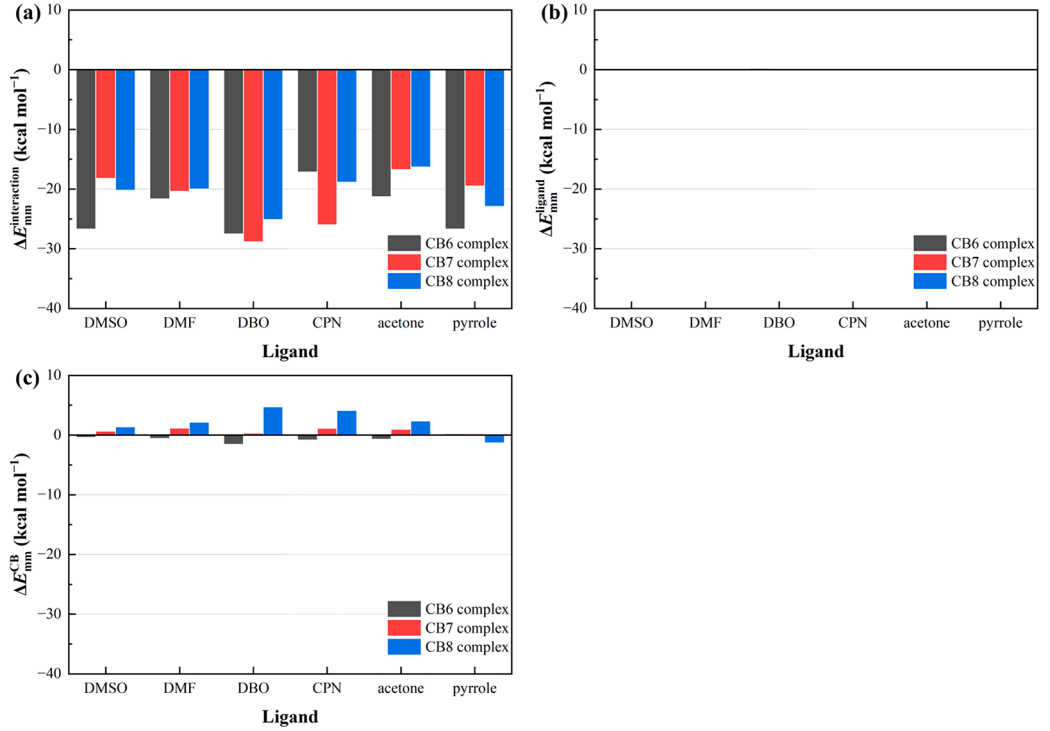

Figure 6. Components of ΔE_{mm} for all combinations of CBs and ligands. (a) The intersolute interaction energy, $\Delta E_{mm}^{interaction}$, and the structural energy changes of (b) ligands ΔE_{mm}^{ligand} and (c) CBs ΔE_{mm}^{CB}. All the values are given in kcal mol^{-1}.

C═O functional groups in the glycoluril units are highly polarized (see Table S1) and may be electrostatically stabilized upon interaction with the solvent water. Figure 4c shows an increasing PMV, reflecting the molecular weight increase.

The SFEs of ligand molecules are also shown in Figure 4b. The DMSO and DMF show favorable SFEs. The larger dipole moment of DMSO and DMF contributes to greater stabilization in the solvent water. The other four ligands show similar SFEs: about −10 kcal mol^{-1}. However, PMV values of DBO and CPN are greater than those for the other ligand molecules, depending on the number of contained atoms.

https://doi.org/10.1021/acs.jpcb.3c00343
J. Phys. Chem. B 2023, 127, 3651−3662

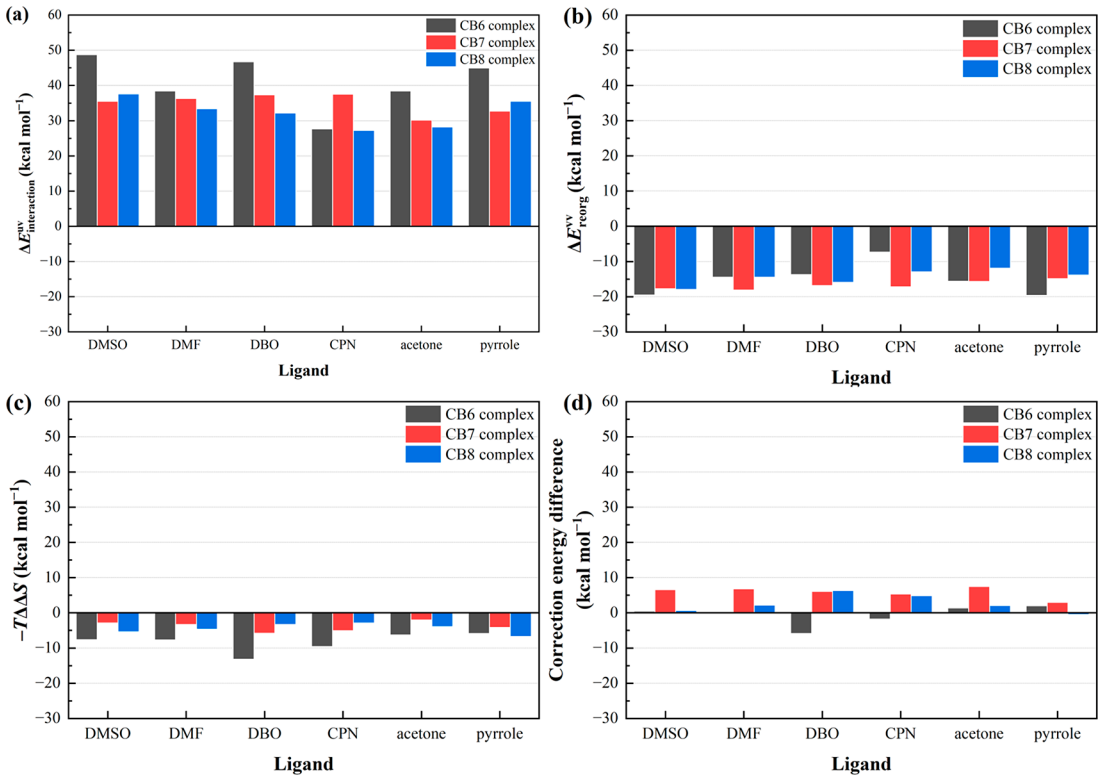

Figure 7. Components of ΔG_{solv} for all combinations of CBs and ligands. (a) The solute−solvent interaction energy, $\Delta E^{uv}_{interaction}$, (b) the solvent reorganization energy, ΔE^{vv}_{reorg}, (c) the solvation entropy change, $-T\Delta\Delta S$, and (d) the pressure correction term. All the values are given in kcal mol^{-1}.

These factors play an essential role in determining the binding affinity to CB, as discussed below.

3.2. Binding Free Energy. The binding free energies of CB*n* with ligand molecules in aqueous solution are now discussed. In Figure 5, the binding free energy and its components are plotted for all the combinations of CB*n* and ligands. The effect of CB size on the binding affinity is a distinctive characteristic, depending on the ligand molecule. For solvents DMSO, DMF, acetone, and pyrrole, CB6 has a greater affinity than CB7, while for DBO and CPN, CB7 has a greater affinity than CB8. These behaviors qualitatively agree with results of earlier experiments.[18] To assess the accuracy of the binding free energy obtained here, we also compared the 3D-RISM results with the calculated binding free energy via other methods, i.e., Molecular Mechanics/Poisson−Boltzmann Surface Area (MM/PBSA) and Molecular Mechanics/Generalized Born Surface Area (MM/GBSA). The results are shown in Figure S3. The qualitative trends are almost the same for all the methods. In addition, the 3D-RISM and MM/PBSA show similar quantitative results, although the MM/GBSA shows greater stabilization compared with the other methods. In Figure S4, the computational results are also compared with the experimental results.[18] The 3D-RISM and MM/PBSA results achieve a good correlation with the experimental data, and therefore, the 3D-RISM data obtained in this study are considered to be reasonable.

In all cases, ΔG_{bind} and ΔE_{mm} are negative, whereas ΔG_{solv} is positive. The components of ΔE_{mm} given in eq 3 can be rewritten as

$$\Delta E_{mm} = \Delta E^{interaction}_{mm} + \Delta E^{ligand}_{mm} + \Delta E^{CB}_{mm} \quad (7)$$

where $\Delta E^{interaction}_{mm}$, ΔE^{ligand}_{mm}, and ΔE^{CB}_{mm} are the CB−ligand interaction energy, and structural energy changes of the ligand and the CB due to the binding, respectively. These components are plotted in Figure 6.

At a glance, $\Delta E^{interaction}_{mm}$ can be recognized as a major component; the contributions of structural energy changes ΔE^{ligand}_{mm} and ΔE^{CB}_{mm} are limited. Only ΔE^{CB}_{mm} of CB8 shows a relatively large contribution, although still small compared with $\Delta E^{interaction}_{mm}$. These results imply that the structural change due to binding is very small. The CB size dependence of $\Delta E^{interaction}_{mm}$ show different tendencies for the different ligands. The smaller ligands (DMSO, DMF, acetone, and pyrrole) show greater stabilization in terms of $\Delta E^{interaction}_{mm}$ for CB6, whereas the larger ligands (DBO and CPN) show greater stabilization for CB7.

ΔG_{solv} can also be split into three components, as follows:

$$\Delta G_{solv} = \Delta E^{uv}_{interaction} + \Delta E^{vv}_{reorg} - T\Delta\Delta S \quad (8)$$

where $\Delta E^{uv}_{interaction}$, ΔE^{vv}_{reorg}, and $-T\Delta\Delta S$ are the solute−solvent interaction energy, solvent reorganization energy, and solvation entropy changes, respectively.[70]

$\Delta E^{uv}_{interaction}$ is given by

$$\Delta E^{uv}_{interaction} = \sum_{\alpha} \rho_{\alpha} \int u_{\alpha}(\boldsymbol{r}) g_{\alpha}(\boldsymbol{r})\, d\boldsymbol{r} \quad (9)$$

and the solvation entropy term is evaluated by the numerical differentiation of the SFE with respect to temperature.

The solvent reorganization energy is obtained from $\Delta E^{vv}_{reorg} = \Delta G_{solv} - \Delta E^{uv}_{interaction} + T\Delta\Delta S$. In addition, we employed the pressure correction method[34,38] as a correction term. Consequently, ΔG_{solv} has four components; they are plotted in Figure 7. $\Delta E^{uv}_{interaction}$ has a positive value, whereas the

https://doi.org/10.1021/acs.jpcb.3c00343
J. Phys. Chem. B 2023, 127, 3651−3662

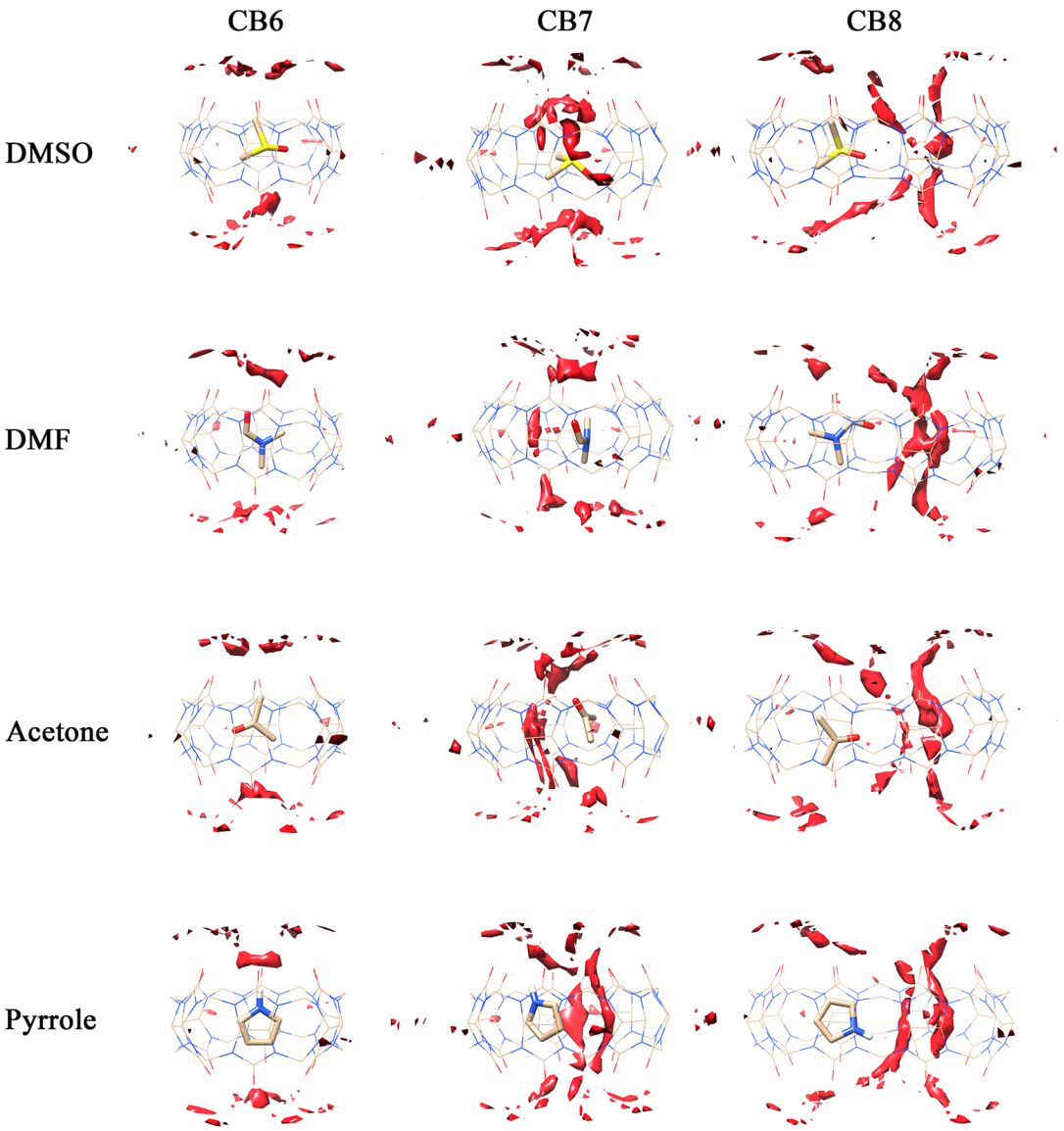

Figure 8. Solvation structures of CB−DMSO/DMF/acetone/pyrrole complexes. Isosurfaces of water oxygen distribution, $g_O(r) = 4.0$, are depicted in red.

solvation entropy and solvent reorganization energy terms are negative. The dehydration of both the ligands and the CBs due to the binding contributes to a decrease in the solute−solvent interaction energy—this is a reason for the positive values of $\Delta E^{uv}_{interaction}$. At the same time, the solvent water released from the CB cavity acquires translational entropy and stabilizes by reorganization of the hydrogen bond network. These energy gains correspond to the "high-energy water" concept reported in earlier studies.[18,19] For DMF, DBO, and acetone, $\Delta E^{uv}_{interaction}$ decreases slightly with increasing CB size—CB7 shows the highest value for CPN and the lowest for DMSO and pyrrole. Here, the reorganization energy and the solvation entropy terms show similar trends but have opposite signs.

The host−ligand direct interaction $\Delta E^{interaction}_{mm}$, the release of "high-energy water" ΔE^{vv}_{reorg}, and $-T\Delta\Delta S$ can be regarded as driving forces of ligand binding. The CB size dependence of the components of binding free energy differs depending on the specific ligands (mentioned above). Based on these characteristics, ligands can be divided into two types: small ligands (DMSO, DMF, acetone, and pyrrole) and larger ligands (DBO and CPN). The following subsections provide a detailed discussion of each type.

3.2.1. Small Ligands. In the case of DMSO, CB6 shows the greatest ligand affinity and CB7 the lowest. This greater stabilization of DMSO binding to the CB6 is attributed to the large ΔE_{mm} stabilization, compared with CB7 and CB8; it mainly originates from the intermolecular interaction between CB6 and DMSO (see Figure 6a). The representative CB−ligand complex structures and the solvation structures are depicted in Figure 8. The solvation structures of ligand unbound CBs are depicted in Figure S5. As seen in the former figure, the DMSO is bound to the center of the CB6 cavity and the water molecules inside the cavity are completely expelled. This means that the DMSO ligand fits well into the CB6 cavity; thus, the DMSO−CB6 can interact strongly. The dehydration of the CB6 cavity and the ligand DMSO itself contributes to the energy penalty on the solute−solvent interaction energy $\Delta E^{uv}_{interaction}$ shown in Figure 7a. In the case of CB7, the binding free energy ΔG_{bind} is slightly higher than in the case of CB6. This is a result of change in the binding

https://doi.org/10.1021/acs.jpcb.3c00343
J. Phys. Chem. B 2023, 127, 3651−3662

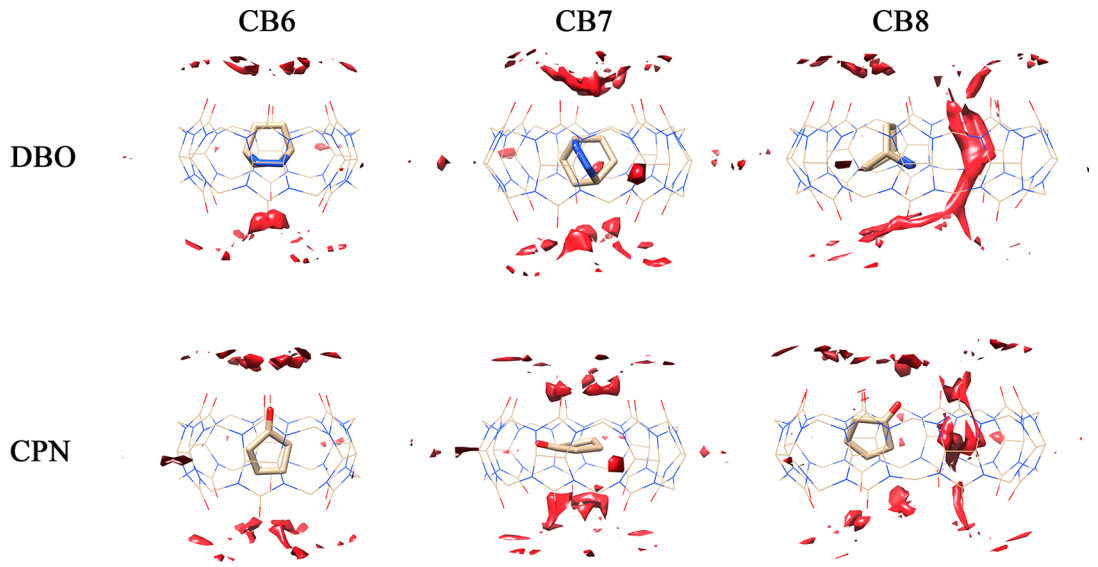

Figure 9. Solvation structures of CB−DBO/CPN complexes. Isosurfaces of water oxygen distribution, $g_O(r) = 4.0$, are depicted in red.

conformation of DMSO. In Figure 8, the water distribution can be found inside the CB7 cavity, unlike in CB6. This indicates that dehydration of the CB7 cavity is incomplete due to the loose fit of DMSO into the CB7 cavity. Consequently, $\Delta E_{mm}^{interaction}$ is about 8.6 kcal mol^{-1} higher and ΔG_{solv} is about 6.7 kcal mol^{-1} lower than in the case of CB6. For CB8, ΔG_{bind} of the DMSO shows a medium value, between that of CB6 and CB7.

As mentioned earlier, the form of CB8 without ligands can fluctuate—it can take both elliptical and circular forms. Figure S6 shows CB8 taking both elliptical and circular forms upon creation of the CB8−DMSO complex. (In the figure, the elliptical and circular forms correspond to large and small RMSD values, respectively.) In Figure S7, representative snapshots of the CB8−ligand complex structures are depicted. In both cases, the cavity of CB8 is large enough to contain the DMSO; therefore, the partial dehydration occurs in a similar fashion to in CB7, as shown in Figure 8. The behavior of the components of ΔG_{bind} is very similar to that in CB7—the numerical difference is only a few kcal mol^{-1}.

The DMF and acetone cases also exhibit basically the same behavior as the DMSO case, although the order of affinity of CB7 and CB8 is inverted from that of the DMSO case. By contrast, the pyrrole shows a different feature for the CB size dependence on the binding affinity—CB8 has a greater affinity than CB6. The ΔE_{mm} value of a CB8−pyrrole complex is similar to that of a CB6−pyrrole complex, but ΔG_{solv} of the CB8−pyrrole complex is much lower than that of the CB6−pyrrole complex. In other words, the pyrrole is strongly stabilized by the interaction with CB8, as in the CB6 case, but the dehydration penalty due to the binding is much lower. The RMSD plot of the CB8−pyrrole complex also shows unique behavior (see Figure S6). The CB8-bound pyrrole takes only an elliptical form, unlike with the other small ligands. This feature may be attributed to the hydrophobicity of the pyrrole molecule. As is evident from Table 1, pyrrole has a positive log K_{ow} value and relatively low dipole moment. Therefore, the elliptical form, which offers greater dehydration and can interact with the hydrophobic part of the CB cavity, is considered preferable.

3.2.2. Large Ligands. The DBO and CPN ligands have relatively large molecular sizes (see Figure 4d). These two ligands show greater affinities for the CB7 than the other CBs. Although the CB size dependence of the total ΔG_{bind} is qualitatively the same for these two ligands, there are different trends in the component of ΔG_{bind}. In the cases of CB6 and CB7, ΔE_{mm} is very close for the DBO ligand, whereas ΔE_{mm} of CB6 for the CPN ligand is higher than that of CB7. In both cases, ΔE_{mm} of CB8 is higher than those of CB6 and CB7. ΔG_{solv} also exhibits a different feature: it gradually decreases with increasing CB size for DBO; ΔG_{solv} of CB7 has the highest value for CPN. To address these differences, the solvation structures of CB−ligand complex structures are depicted in Figure 9, and the superposition representation of complex structures is depicted in Figure S8.

For the DBO ligand, no water distribution was found inside the cavities of CB6 and CB7, unlike in CB8 (see Figure 9). Indications are that the DBO fits into both the CB6 and CB7 cavities, resulting in complete dehydration via complex formation. These tight-fit bindings create greater stabilization in $\Delta E_{mm}^{interaction}$. $\Delta E_{mm}^{interaction}$ of CB6 is slightly higher than that of CB7, but the total ΔE_{mm} is comparable due to the conformational stabilization contribution of ΔE_{mm}^{CB} of CB6 upon binding. ΔG_{solv} of DBO gradually decreases with increasing CB size. CB8 has the lowest dehydration penalty because it remains partially hydrated. Both CB6 and CB7 are fully dehydrated; however, as seen in Figure S5, CB6 should pay a higher dehydration penalty because of the stronger solvent distribution in CB6.

For the CPN ligand, solvation structures are similar to the DBO cases; no water distribution was found inside the cavities of CB6 and CB7, unlike in CB8. $\Delta E_{mm}^{interaction}$ of CB6 is about 8.8 kcal mol^{-1} higher than that of CB7. In Figure S8, CPN shows a characteristic orientation in CB6 and CB7, while DBO shows a random orientation. Specifically, the molecular axis of the ligand is oriented in the direction of the axis of rotation of the CB6, whereas it is perpendicular to the axis of rotation of the CB7. This suggests that the ligands are oriented only in a specific direction because the cavity size is not large enough in CB6. Therefore, $\Delta E_{mm}^{interaction}$ of CB6 is presumably higher than that of CB7 because of the repulsive interaction between the

https://doi.org/10.1021/acs.jpcb.3c00343
J. Phys. Chem. B 2023, 127, 3651−3662

ligand and the CB due to the tight fit into the cavity. ΔG_{solv} of CPN and DBO show different trends. ΔG_{solv} of the CB6−CPN complex is lower than that of CB7−CPN. In Figure 7a, $\Delta E^{uv}_{interaction}$ of CB6 is lower than that of CB7, meaning that the dehydration penalty of the CB6 complex is lower. In Figure S9, the solvation structure of the CB6−CPN complex is depicted. There it is seen that the carbonyl oxygen of the ligand forms a hydrogen bond with the solvent water. CPN retains hydrogen bonds after complex formation, contributing to the reduction of the dehydration penalty. By contrast, CPN in CB7 is not oriented with the carboxyl groups facing out of the cavity; hence, such hydrogen bonds cannot form.

These results show that even ligands of similar size exhibit completely different CB size dependence due to the different binding structures in the cavities.

4. CONCLUSIONS

The role of water in the binding of six ligands to three types of CBs (CB6, CB7, and CB8) was investigated using the 3D-RISM theory and MD simulation. From the binding free energy and its components, the ligands were divided into two types: relatively small ligands, namely DMSO, DMF, acetone, and pyrrole, and relatively larger ligands, namely DBO and CPN.

In the case of the small ligands, the solvent water is released from the CB6 cavity and the cavity is fully dehydrated, whereas the CB7 and CB8 retain hydration water in their cavities after complex formation. This indicates that these small ligands fit well into the cavity of CB6. They exhibit greater affinity compared with the larger CBs, except in the case of the pyrrole ligand. The pyrrole is strongly stabilized by the interaction with CB8, as in the CB6 case—the CB8-bound pyrrole takes an elliptical form—however, the dehydration penalty due to the binding is much lower. This is the cause of the characteristic CB size dependence of the binding affinity of pyrrole.

In the case of the large ligands, no water distribution was found in the CB6 and CB7 cavities. This indicates that DBO and CPN fit into both the CB6 and CB7 cavities. Although these two ligands exhibit similar CB size dependencies of binding affinity, the tendencies of the binding affinity components are completely different. The reason for the difference arises from the difference between the complex structure and the subsequent solvation structure.

Prediction of ligand affinity by CBs is a target of SAMPL8, which has received the most attention in evaluating the predictive performance of molecular recognition processes.[71] Although the size-dependent affinity of CBs for specific ligands was examined in this paper, the method is expected to be applicable to a wide range of ligands, as shown in SAMPL8. Our findings are expected to contribute to a deeper understanding of the CB binding affinity and to the development of ligand design.

■ ASSOCIATED CONTENT

Supporting Information

The Supporting Information is available free of charge at https://pubs.acs.org/doi/10.1021/acs.jpcb.3c00343.

Computational details of the MM/PBSA and MM/GBSA calculations, the force field parameters, RMSD of MD trajectories, MM/PBSA and MM/GBSA energies, comparison with the experimental data, energy components of CB8, additional solvation structure, and complex structures (PDF)

■ AUTHOR INFORMATION

Corresponding Authors

Piyarat Nimmanpipug − *Department of Chemistry, Faculty of Science, Chiang Mai University, Chiang Mai 50200, Thailand;* orcid.org/0000-0001-6364-504X; Email: piyarat.n@cmu.ac.th

Norio Yoshida − *Department of Complex Systems Science, Graduate School of Informatics, Nagoya University, Nagoya 464-8601, Japan;* orcid.org/0000-0002-2023-7254; Email: noriwo@nagoya-u.jp

Authors

Natthiti Chiangraeng − *Department of Chemistry, Graduate School of Science, Kyushu University, Fukuoka 819-0395, Japan; Department of Chemistry, Faculty of Science, Chiang Mai University, Chiang Mai 50200, Thailand;* orcid.org/0000-0002-6141-7067

Haruyuki Nakano − *Department of Chemistry, Graduate School of Science, Kyushu University, Fukuoka 819-0395, Japan;* orcid.org/0000-0002-7008-0312

Complete contact information is available at: https://pubs.acs.org/10.1021/acs.jpcb.3c00343

Author Contributions

The authors confirm the following contributions to this paper. Study conception and design: N.C., P.N., and N.Y. Data collection: N.C. and N.Y. Analysis and interpretation of results: N.C. and N.Y. Draft manuscript preparation: N.C., H.N., P.N., and N.Y. All authors reviewed the results and approved the final version of the manuscript.

Funding

This study was financially supported by the Japan Society for the Promotion of Science (JSPS) KAKENHI (Grant Nos. 19H02677 and 22H05089). P.N. and N.C. acknowledge financial support from the Fundamental Fund, Chiang Mai University (CMU). N.C. thanks the Science Achievement Scholarship of Thailand (SAST) for the visiting fund at Kyushu University.

Notes

The authors declare no competing financial interest.

■ ACKNOWLEDGMENTS

Numerical calculations were partially conducted at the Research Center for Computational Science, Institute for Molecular Science, National Institutes of Natural Sciences (Project: 22-IMS-C076) and using MCRP-S at the Center for Computational Science, University of Tsukuba. Molecular graphics were produced from Chimera.[72] We also acknowledge Ms. Sakurae for preliminary computations.

■ ABBREVIATIONS

3D-RISM,three-dimensional reference interaction site model; CB*n*,cucurbit[*n*]uril; CPN,cyclopentanone; DBO,2,3-diazabicyclo[2.2.2]oct-2-ene; DMF,*N*,*N*-dimethylformamide; DMSO,dimethyl sulfoxide; GAFF,general Amber force field; KH,Kovalenko−Hirata; MD,molecular dynamics; MR,molecular recognition; PMV,partial molar volume or $\Delta\bar{V}$; RMSD,root-mean-square deviation; SFE,solvation free energy.

https://doi.org/10.1021/acs.jpcb.3c00343
J. Phys. Chem. B 2023, 127, 3651−3662

REFERENCES

(1) Lagona, J.; Mukhopadhyay, P.; Chakrabarti, S.; Isaacs, L. The Cucurbit[n]Uril Family. *Angew. Chem. Int. Ed.* **2005**, *44* (31), 4844−4870.

(2) Barrow, S. J.; Kasera, S.; Rowland, M. J.; del Barrio, J.; Scherman, O. A. Cucurbituril-Based Molecular Recognition. *Chem. Rev.* **2015**, *115* (22), 12320−12406.

(3) Yoshida, N. Role of Solvation in Drug Design as Revealed by the Statistical Mechanics Integral Equation Theory of Liquids. *J. Chem. Inf. Model.* **2017**, *57* (11), 2646−2656.

(4) Pandya, J. B.; Shinde, S. M.; Jha, P. K. Theoretical Study on the Interaction of Flutamide Anticancer Drug with Cucurbit[n]Uril (*n* = 5−8) as a Drug Delivery System. *Int. J. Quantum Chem.* **2022**, *122* (12), e26899.

(5) Li, C. Pillararene-Based Supramolecular Polymers: From Molecular Recognition to Polymeric Aggregates. *Chem. Commun.* **2014**, *50* (83), 12420−12433.

(6) Harada, A.; Kobayashi, R.; Takashima, Y.; Hashidzume, A.; Yamaguchi, H. Macroscopic Self-Assembly through Molecular Recognition. *Nat. Chem.* **2011**, *3* (1), 34−37.

(7) Chang, H.-Y.; Wu, K.-Y.; Chen, W.-C.; Weng, J.-T.; Chen, C.-Y.; Raj, A.; Hamaguchi, H.; Chuang, W.-T.; Wang, X.; Wang, C.-L. Water-Induced Self-Assembly of Amphiphilic Discotic Molecules for Adaptive Artificial Water Channels. *ACS Nano* **2021**, *15* (9), 14885−14890.

(8) Harano, Y.; Kinoshita, M. Large Gain in Translational Entropy of Water Is a Major Driving Force in Protein Folding. *Chem. Phys. Lett.* **2004**, *399* (4), 342−348.

(9) Bhosle, A. A.; Banerjee, M.; Barooah, N.; Bhasikuttan, A. C.; Kadu, K.; Ramanan, S. R.; Chatterjee, A. ESIPT-Active Hydroxybenzothiazole-Picolinium@CB[7]-HAp NPs Based Supramolecular Sensing Assembly for Spermine, Spermidine and Cadaverine: Application in Monitoring Cancer Biomarkers and Food Spoilage. *J. Photochem. Photobiol. A Chem.* **2022**, *426*, 113770.

(10) Al Tbakhi, B.; Nsairat, H.; Alshaer, W.; Al-Kadash, A.; Helal, W.; Alrawashdeh, L.; Day, A.; Assaf, K. I.; Hassouneh, R.; Odeh, F.; Al Bawab, A. Cinnamaldehyde-Cucurbituril Complex: Investigation of Loading Efficiency and Its Role in Enhancing Cinnamaldehyde in Vitro Anti-Tumor Activity. *RSC Adv.* **2022**, *12* (12), 7540−7549.

(11) Hettiarachchi, G.; Nguyen, D.; Wu, J.; Lucas, D.; Ma, D.; Isaacs, L.; Briken, V. Toxicology and Drug Delivery by Cucurbit[n]-Uril Type Molecular Containers. *PLoS One* **2010**, *5* (5), e10514.

(12) Zhang, X.; Xu, X.; Li, S.; Wang, L.-H.; Zhang, J.; Wang, R. A Systematic Evaluation of the Biocompatibility of Cucurbit[7]Uril in Mice. *Sci. Rep.* **2018**, *8* (1), 8819.

(13) Uzunova, V. D.; Cullinane, C.; Brix, K.; Nau, W. M.; Day, A. I. Toxicity of Cucurbit[7]Uril and Cucurbit[8]Uril: An Exploratory in Vitro and in Vivo Study. *Org. Biomol. Chem.* **2010**, *8* (9), 2037−2042.

(14) Aktanova, A.; Abramova, T.; Pashkina, E.; Boeva, O.; Grishina, L.; Kovalenko, E.; Kozlov, V. Assessment of the Biocompatibility of Cucurbiturils in Blood Cells. *Nanomaterials* **2021**, *11* (6), 1356.

(15) Oun, R.; Floriano, R. S.; Isaacs, L.; Rowan, E. G.; Wheate, N. J. The Ex Vivo Neurotoxic, Myotoxic and Cardiotoxic Activity of Cucurbituril-Based Macrocyclic Drug Delivery Vehicles. *Toxicol. Res. (Camb).* **2014**, *3* (6), 447−455.

(16) Walker, S.; Oun, R.; McInnes, F. J.; Wheate, N. J. The Potential of Cucurbit[n]Urils in Drug Delivery. *Isr. J. Chem.* **2011**, *51* (5−6), 616−624.

(17) Sin, K. R.; Kim, C. J.; Ko, S. G.; Hwang, T. M.; Han, Y. N.; Pak, Y. N. Inclusion of Thymol into Cucurbiturils: Density Functional Theory Approach with Dispersion Correction and Natural Bond Orbital Analysis. *J. Incl. Phenom. Macrocycl. Chem.* **2022**, *102* (5), 533−542.

(18) Biedermann, F.; Uzunova, V. D.; Scherman, O. A.; Nau, W. M.; De Simone, A. Release of High-Energy Water as an Essential Driving Force for the High-Affinity Binding of Cucurbit[n]Urils. *J. Am. Chem. Soc.* **2012**, *134* (37), 15318−15323.

(19) Biedermann, F.; Vendruscolo, M.; Scherman, O. A.; De Simone, A.; Nau, W. M. Cucurbit[8]Uril and Blue-Box: High-Energy Water Release Overwhelms Electrostatic Interactions. *J. Am. Chem. Soc.* **2013**, *135* (39), 14879−14888.

(20) Assaf, K. I.; Florea, M.; Antony, J.; Henriksen, N. M.; Yin, J.; Hansen, A.; Qu, Z. W.; Sure, R.; Klapstein, D.; Gilson, M. K.; Grimme, S.; Nau, W. M. HYDROPHOBE Challenge: A Joint Experimental and Computational Study on the Host-Guest Binding of Hydrocarbons to Cucurbiturils, Allowing Explicit Evaluation of Guest Hydration Free-Energy Contributions. *J. Phys. Chem. B* **2017**, *121* (49), 11144−11162.

(21) Grimm, L. M.; Spicher, S.; Tkachenko, B.; Schreiner, P. R.; Grimme, S.; Biedermann, F. The Role of Packing, Dispersion, Electrostatics, and Solvation in High-Affinity Complexes of Cucurbit-[n]Urils with Uncharged Polar Guests. *Chem. A Eur. J.* **2022**, *28* (38), No. e202200529.

(22) Yoshida, N.; Imai, T.; Phongphanphanee, S.; Kovalenko, A.; Hirata, F. Molecular Recognition in Biomolecules Studied by Statistical-Mechanical Integral-Equation Theory of Liquids. *J. Phys. Chem. B* **2009**, *113* (4), 873−886.

(23) Kovalenko, A.; Hirata, F. Self-Consistent Description of a Metal-Water Interface by the Kohn-Sham Density Functional Theory and the Three-Dimensional Reference Interaction Site Model. *J. Chem. Phys.* **1999**, *110* (20), 10095−10112.

(24) Kovalenko, A.; Hirata, F. Potential of Mean Force between Two Molecular Ions in a Polar Molecular Solvent: A Study by the Three-Dimensional Reference Interaction Site Model. *J. Phys. Chem. B* **1999**, *103* (37), 7942−7957.

(25) Hirata, F. *Molecular Theory of Solvation*; Kluwer: Dordrecht, The Netherlands, 2003.

(26) Roux, B.; Yu, H. A.; Karplus, M. Molecular Basis for the for the Born Model of Ion Solvation. *J. Phys. Chem.* **1990**, *94* (11), 4683−4688.

(27) Chandler, D.; McCoy, J. D.; Singer, S. J. Density Functional Theory of Nonuniform Polyatomic Systems. I. General Formulation. *J. Chem. Phys.* **1986**, *85* (10), 5971−5976.

(28) Kovalenko, A.; Hirata, F. Three-Dimensional Density Profiles of Water in Contact with a Solute of Arbitrary Shape: A RISM Approach. *Chem. Phys. Lett.* **1998**, *290* (1−3), 237−244.

(29) Singer, S. J.; Chandler, D. Free Energy Functions in the Extended RISM Approximation. *Mol. Phys.* **1985**, *55* (3), 621−625.

(30) Sugita, M.; Onishi, I.; Irisa, M.; Yoshida, N.; Hirata, F. Molecular Recognition and Self-Organization in Life Phenomena Studied by a Statistical Mechanics of Molecular Liquids, the RISM/3D-RISM Theory. *Molecules* **2021**, *26* (2), 271.

(31) Imai, T. Molecular Theory of Partial Molar Volume and Its Applications to Biomolecular Systems. *Condens. Matter Phys.* **2007**, *10* (3), 343−361.

(32) Palmer, D. S.; Frolov, A. I.; Ratkova, E. L.; Fedorov, M. V. Towards a Universal Method for Calculating Hydration Free Energies: A 3D Reference Interaction Site Model with Partial Molar Volume Correction. *J. Phys.: Condens. Matter* **2010**, *22* (49), 492101.

(33) Truchon, J.-F.; Pettitt, B. M.; Labute, P. A Cavity Corrected 3D-RISM Functional for Accurate Solvation Free Energies. *J. Chem. Theory Comput.* **2014**, *10* (3), 934−941.

(34) Sergiievskyi, V.; Jeanmairet, G.; Levesque, M.; Borgis, D. Solvation Free-Energy Pressure Corrections in the Three Dimensional Reference Interaction Site Model. *J. Chem. Phys.* **2015**, *143* (18), 184116.

(35) Misin, M.; Fedorov, M. V.; Palmer, D. S. Communication: Accurate Hydration Free Energies at a Wide Range of Temperatures from 3D-RISM. *J. Chem. Phys.* **2015**, *142* (9), 091105.

(36) Roy, D.; Blinov, N.; Kovalenko, A. Predicting Accurate Solvation Free Energy in N-Octanol Using 3D-RISM-KH Molecular Theory of Solvation: Making Right Choices. *J. Phys. Chem. B* **2017**, *121* (39), 9268−9273.

(37) Huang, W.; Blinov, N.; Kovalenko, A. Octanol−Water Partition Coefficient from 3D-RISM-KH Molecular Theory of Solvation with Partial Molar Volume Correction. *J. Phys. Chem. B* **2015**, *119* (17), 5588−5597.

https://doi.org/10.1021/acs.jpcb.3c00343
J. Phys. Chem. B 2023, 127, 3651−3662

(38) Tanimoto, S.; Yoshida, N.; Yamaguchi, T.; Ten-No, S. L.; Nakano, H. Effect of Molecular Orientational Correlations on Solvation Free Energy Computed by Reference Interaction Site Model Theory. *J. Chem. Inf. Model.* **2019**, *59* (9), 3770−3781.
(39) Tielker, N.; Güssregen, S.; Kast, S. M. SAMPL7 Physical Property Prediction from EC-RISM Theory. *J. Comput. Aided. Mol. Des.* **2021**, *35* (8), 933−941.
(40) Tielker, N.; Tomazic, D.; Eberlein, L.; Güssregen, S.; Kast, S. M. The SAMPL6 Challenge on Predicting Octanol−Water Partition Coefficients from EC-RISM Theory. *J. Comput. Aided. Mol. Des.* **2020**, *34* (4), 453−461.
(41) Luchko, T.; Blinov, N.; Limon, G. C.; Joyce, K. P.; Kovalenko, A. SAMPL5:3D-RISM Partition Coefficient Calculations with Partial Molar Volume Corrections and Solute Conformational Sampling. *J. Comput. Aided. Mol. Des.* **2016**, *30* (11), 1115−1127.
(42) Roy, D.; Kovalenko, A. Evaluating Performance of the Approximate 3D-RISM-KH Molecular Solvation Theory for Solvation Free Energies in Alkanes and Alkane-Water Partition Coefficients. *J. Mol. Liq.* **2023**, *378*, 121597.
(43) Sugita, M.; Hirata, F. Predicting the Binding Free Energy of the Inclusion Process of 2-Hydroxypropyl-β-Cyclodextrin and Small Molecules by Means of the MM/3D-RISM Method. *J. Phys.: Condens. Matter* **2016**, *28* (38), 384002.
(44) Hayashino, Y.; Sugita, M.; Arima, H.; Irie, T.; Kikuchi, T.; Hirata, F. Predicting the Binding Mode of 2-Hydroxypropyl-β-Cyclodextrin to Cholesterol by Means of the MD Simulation and the 3D-RISM-KH Theory. *J. Phys. Chem. B* **2018**, *122* (21), 5716−5725.
(45) Sugita, M.; Kuwano, I.; Higashi, T.; Motoyama, K.; Arima, H.; Hirata, F. Computational Screening of a Functional Cyclodextrin Derivative for Suppressing a Side Effect of Doxorubicin. *J. Phys. Chem. B* **2021**, *125* (9), 2308−2316.
(46) Yoshida, N.; Phongphanphanee, S.; Hirata, F. Selective Ion Binding by Protein Probed with the Statistical Mechanical Integral Equation Theory. *J. Phys. Chem. B* **2007**, *111* (17), 4588−4595.
(47) Yoshida, N.; Kiyota, Y.; Phongphanphanee, S.; Maruyama, Y.; Imai, T.; Hirata, F. Statistical Mechanics Theory of Molecular Recognition and Pharmaceutical Design. *Int. Rev. Phys. Chem.* **2011**, *30* (4), 445−478.
(48) Imai, T.; Kovalenko, A.; Hirata, F. Partial Molar Volume of Proteins Studied by the Three-Dimensional Reference Interaction Site Model Theory. *J. Phys. Chem. B* **2005**, *109* (14), 6658−6665.
(49) Imai, T.; Kovalenko, A.; Hirata, F. Solvation Thermodynamics of Protein Studied by the 3D-RISM Theory. *Chem. Phys. Lett.* **2004**, *395* (1−3), 1−6.
(50) Imai, T.; Kinoshita, M.; Hirata, F. Theoretical Study for Partial Molar Volume of Amino Acids in Aqueous Solution: Implication of Ideal Fluctuation Volume. *J. Chem. Phys.* **2000**, *112* (21), 9469−9478.
(51) Case, D. A.; Belfon, K.; Ben-Shalom, I. Y.; Brozell, S. R.; Cerutti, D. S.; Cheatham, T. E., III; Cruzeiro, V. W. D.; Darden, T. A.; Duke, R. E.; Giambasu, G.; Gilson, M. K.; Gohlke, H.; Goetz, A. W.; Harris, R.; Izadi, S.; Izmailov, S. A.; Kasavajhala, K.; Kovalenko, A.; Krasny, R.; Kurtzman, T.; Lee, T. S.; LeGrand, S.; Li, P.; Lin, C.; Liu, J.; Luchko, T.; Luo, R.; Man, V.; Merz, K. M.; Miao, Y.; Mikhailovskii, O.; Monard, G.; Nguyen, H.; Onufriev, A.; Pan, F.; Pantano, S.; Qi, R.; Roe, D. R.; Roitberg, A.; Sagui, C.; Schott-Verdugo, S.; Shen, J.; Simmerling, C. L.; Skrynnikov, N. R.; Smith, J.; Swails, J.; Walker, R. C.; Wang, J.; Wilson, L.; Wolf, R. M.; Wu, X.; Xiong, Y.; Xue, Y. *Amber 20*; University of California: San Francisco, CA, 2020.
(52) Frisch, M. J.; Trucks, G. W.; Schlegel, H. B.; Scuseria, G. E.; Robb, M. A.; Cheeseman, J. R.; Scalmani, G.; Barone, V.; Petersson, G. A.; Nakatsuji, H.; Li, X.; Caricato, M.; Marenich, A. V; Bloino, J.; Janesko, B. G.; Gomperts, R.; Mennucci, B.; Hratchian, H. P.; Ortiz, J. V; Izmaylov, A. F.; Sonnenberg, J. L.; Williams-Young, D.; Ding, F.; Lipparini, F.; Egidi, F.; Goings, J.; Peng, B.; Petrone, A.; Henderson, T.; Ranasinghe, D.; Zakrzewski, V. G.; Gao, J.; Rega, N.; Zheng, G.; Liang, W.; Hada, M.; Ehara, M.; Toyota, K.; Fukuda, R.; Hasegawa, J.; Ishida, M.; Nakajima, T.; Honda, Y.; Kitao, O.; Nakai, H.; Vreven, T.; Throssell, K.; Montgomery, J. A., Jr.; Peralta, J. E.; Ogliaro, F.; Bearpark, M. J.; Heyd, J. J.; Brothers, E. N.; Kudin, K. N.; Staroverov, V. N.; Keith, T. A.; Kobayashi, R.; Normand, J.; Raghavachari, K.; Rendell, A. P.; Burant, J. C.; Iyengar, S. S.; Tomasi, J.; Cossi, M.; Millam, J. M.; Klene, M.; Adamo, C.; Cammi, R.; Ochterski, J. W.; Martin, R. L.; Morokuma, K.; Farkas, O.; Foresman, J. B.; Fox, D. J. *Gaussian 16*, Rev. C.01; Gaussian, Inc.: Wallingford, CT, 2019.
(53) Wang, J.; Wang, W.; Kollman, P. A.; Case, D. A. Automatic Atom Type and Bond Type Perception in Molecular Mechanical Calculations. *J. Mol. Graph. Model.* **2006**, *25* (2), 247−260.
(54) Wang, J.; Cieplak, P.; Kollman, P. A. How Well Does a Restrained Electrostatic Potential (RESP) Model Perform in Calculating Conformational Energies of Organic and Biological Molecules? *J. Comput. Chem.* **2000**, *21* (12), 1049−1074.
(55) Sangster, J. Octanol-Water Partition Coefficients of Simple Organic Compounds. *J. Phys. Chem. Ref. Data* **1989**, *18* (3), 1111−1229.
(56) Reichardt, C.; Welton, T.. *Solvents and Solvent Effects in Organic Chemistry*, 4th ed.; Wiley−VCH: Weinheim, Germany, 2011.
(57) Reichardt, C. Empirical Parameters of Solvent Polarity as Linear Free-Energy Relationships. *Angew. Chem., Int. Ed. Engl.* **1979**, *18* (2), 98−110.
(58) Famini, G. Using Theoretical Descriptors in Structural Activity Relationships. 1. Molecular Volume. *CRDEC-TR-88031, U.S. Army Chem. Res. Dev. Eng. Cent.*; 1988.
(59) Spafiu, F.; Mischie, A.; Ionita, P.; Beteringhe, A.; Constantinescu, T.; Balaban, A. T. New Alternatives for Estimating the Octanol/Water Partition Coefficient and Water Solubility for Volatile Organic Compounds Using GLC Data (Kovàts Retention Indices). *Arkivoc* **2009**, *2009*, 174−194.
(60) Cerón-Carrasco, J. P.; Jacquemin, D.; Laurence, C.; Planchat, A.; Reichardt, C.; Sraïdi, K. Solvent Polarity Scales: Determination of New $E_T(30)$ Values for 84 Organic Solvents. *J. Phys. Org. Chem.* **2014**, *27* (6), 512−518.
(61) Salomon-Ferrer, R.; Götz, A. W.; Poole, D.; Le Grand, S.; Walker, R. C. Routine Microsecond Molecular Dynamics Simulations with AMBER on GPUs. 2. Explicit Solvent Particle Mesh Ewald. *J. Chem. Theory Comput.* **2013**, *9* (9), 3878−3888.
(62) Götz, A. W.; Williamson, M. J.; Xu, D.; Poole, D.; Le Grand, S.; Walker, R. C. Routine Microsecond Molecular Dynamics Simulations with AMBER on GPUs. 1. Generalized Born. *J. Chem. Theory Comput.* **2012**, *8* (5), 1542−1555.
(63) Le Grand, S.; Götz, A. W.; Walker, R. C. SPFP: Speed without Compromise - A Mixed Precision Model for GPU Accelerated Molecular Dynamics Simulations. *Comput. Phys. Commun.* **2013**, *184* (2), 374−380.
(64) Berendsen, H. J. C.; Postma, J. P. M.; van Gunsteren, W. F.; DiNola, A.; Haak, J. R. Molecular Dynamics with Coupling to an External Bath. *J. Chem. Phys.* **1984**, *81* (8), 3684−3690.
(65) Andersen, H. C. Rattle: A "Velocity" Version of the Shake Algorithm for Molecular Dynamics Calculations. *J. Comput. Phys.* **1983**, *52* (1), 24−34.
(66) Kovalenko, A.; Hirata, F. Potentials of Mean Force of Simple Ions in Ambient Aqueous Solution. II. Solvation Structure from the Three-Dimensional Reference Interaction Site Model Approach, and Comparison with Simulations. *J. Chem. Phys.* **2000**, *112* (23), 10403−10417.
(67) Maruyama, Y.; Yoshida, N.; Tadano, H.; Takahashi, D.; Sato, M.; Hirata, F. Massively Parallel Implementation of 3D-RISM Calculation with Volumetric 3D-FFT. *J. Comput. Chem.* **2014**, *35* (18), 1347−1355.
(68) Yoshida, N. The Reference Interaction Site Model Integrated Calculator (RISMiCal) Program Package for Nano- and Biomaterials Design. *IOP Conf. Ser. Mater. Sci. Eng.* **2020**, *773* (1), No. 012062.
(69) Maruyama, Y.; Hirata, F. Modified Anderson Method for Accelerating 3D-RISM Calculations Using Graphics Processing Unit. *J. Chem. Theory Comput.* **2012**, *8* (9), 3015−3021.
(70) Imai, T.; Harano, Y.; Kinoshita, M.; Kovalenko, A.; Hirata, F. A Theoretical Analysis on Hydration Thermodynamics of Proteins. *J. Chem. Phys.* **2006**, *125* (2), 024911.

https://doi.org/10.1021/acs.jpcb.3c00343
J. Phys. Chem. B 2023, 127, 3651−3662

(71) Amezcua, M.; Setiadi, J.; Ge, Y.; Mobley, D. L. An Overview of the SAMPL8 Host−Guest Binding Challenge. *J. Comput. Aided. Mol. Des.* **2022**, *36* (10), 707−734.
(72) Pettersen, E. F.; Goddard, T. D.; Huang, C. C.; Couch, G. S.; Greenblatt, D. M.; Meng, E. C.; Ferrin, T. E. UCSF Chimera - a Visualization System for Exploratory Research and Analysis. *J. Comput. Chem.* **2004**, *25* (13), 1605−1612.

https://doi.org/10.1021/acs.jpcb.3c00343
J. Phys. Chem. B 2023, 127, 3651−3662